The receptor subunit Tom20 is dynamically associated with the TOM complex in mitochondria of human cells

Maniraj Bhagawati[a,b,c,†], Tasnim Arroum[a,†], Niklas Webeling[a], Ayelén González Montoro[c,d], Henning D. Mootz[b], and Karin B. Busch[a,*]

[a]Department of Biology, Institute of Molecular Cell Biology, and [b]Department of Chemistry and Pharmacy, Institute of Biochemistry, University of Münster, 48149 Münster, Germany; [c]Center of Cellular Nanoanalytics Osnabrück, 49076 Osnabrueck, Germany; [d]Cellular Communication Laboratory, Department of Biology and Chemistry, University of Osnabrueck, 49076 Osnabrueck, Germany

ABSTRACT **The outer membrane translocase (TOM) is the import channel for nuclear-encoded mitochondrial proteins. The general import pore contains Tom40, Tom22, Tom5, Tom6, and Tom7. Precursor proteins are bound by the (peripheral) receptor proteins Tom20, Tom22, and Tom70 before being imported by the TOM complex. Here we investigated the association of the receptor Tom20 with the TOM complex. Tom20 was found in the TOM complex, but not in a smaller subcomplex. In addition, a subcomplex was found without Tom40 and Tom7 but with Tom20. Using single particle tracking of labeled Tom20 in overexpressing human cells, we show that Tom20 has, on average, higher lateral mobility in the membrane than Tom7/TOM. After ligation of Tom20 with the TOM complex by post-tranlational protein trans-splicing using the traceless, ultrafast cleaved Gp41-1 integrin system, a significant decrease in the mean diffusion coefficient of Tom20 was observed in the resulting Tom20–Tom7 fusion protein. Exposure of Tom20 to high substrate loading also resulted in reduced mobility. Taken together, our data show that the receptor subunit Tom20 interacts dynamically with the TOM core complex. We suggest that the TOM complex containing Tom20 is the active import pore and that Tom20 is associated when substrate is available.**

Monitoring Editor
Martin Ott
University of Gothenburg

Received: Feb 1, 2021
Revised: Jul 21, 2021
Accepted: Jul 30, 2021

INTRODUCTION

The translocase of the outer mitochondrial membrane (TOM) is the import channel for more than 99% of the 800–1500 nuclear-encoded mitochondrial proteins (Meisinger *et al.*, 1999; Mootha *et al.*, 2003). The core TOM is also named the general import pore (GIP), which consists of the central channel formed by the β-barrel protein Tom40 and the smaller α-helical membrane proteins Tom7, Tom5 and Tom6, and Tom22 (Ahting *et al.*, 1999; Shiota *et al.*, 2015; Bausewein *et al.*, 2017; Wang *et al.*, 2020). The GIP forms a

This article was published online ahead of print in MBoC in Press (http://www.molbiolcell.org/cgi/doi/10.1091/mbc.E21-01-0042).

†These authors contributed equally.

Conflicts of interest: The authors declare no conflict of interest.

Data availability statement: data are available on request.

Author contributions: conceptualization: K.B.B, M.B., T.A., A.G.M., and H.M.; methodology: K.B.B., N.W., T.A., M.B., A.G.M., and H.M.; validation: K.B.B., M.B., T.A., and A.G.M.; formal analysis: K.B.B., M.B., T.A., N.W., and A.G.M.; investigation: K.B.B., M.B., T.A., and A.G.M.; resources: K.B.B. and A.G.M.; writing—original draft preparation: K.B.B.; writing—review and editing: K.B.B., M.B., and H.M; visualization: T.A., M.B., A.G.M., and K.B.B.; supervision: K.B.B.; project administration: K.B.B.; funding acquisition: K.B.B. and H.M. All authors have read and agreed to the published version of the manuscript.

*Address correspondence to: Karin B. Busch (buschkar@uni-muenster.de).

Abbreviations used: CDF, cumulative density function; FLIM, fluorescence lifetime imaging microscopy; FP, fluorescent protein; FRET, Foerster resonance energy transfer; GIP, general import pore; HT, Halo7-Tag; HTL, Halo-tag ligand; MPP, mitochondrial processing peptidase; MSD, mean-square dispacement; MTDR, MitoTracker Deep Red; mts, matrix-targeting sequence; N.A., numerical aperture; OMM, outer mitochondrial membrane; PDF, probability density function; PTS, Protein trans-splicing; PVDF, polyvinylidene fluoride; SC, supercomplex; sEcGFP, supereclipticic green fluorescent protein; SiR, silico rhodamine; SMT, Single molecule tracking; SPT, single particle tracking; TIRF, total internal reflection fluorescence; TCSPC, time-correlated single photon counting; TIM, translocase of the inner membrane; TMR, tetramethyl rhodamine; TOM, translocase of the outer membrane; VDAC, voltage-dependent anion channel; WWL, white light laser.

symmetrical dimer or trimer (Bausewein *et al.*, 2017; Sakaue *et al.*, 2019) of ~490–600 kDa (Ahting *et al.*, 1999). It is suggested that the different assembly forms (dimeric, trimeric, and also tetrameric) have different functions, for example, the dimer is an assembly state, respectively, and is involved in the transfer of intermembrane space proteins, while the trimer is the protein translation state (Gornicka *et al.*, 2014; Araiso *et al.*, 2020). The TOM complex is fully embedded in the lipid bilayer of the outer mitochondrial membrane (OMM). Recent high resolution cryo-EM data show that monomeric fungal (PDB ID, 6JNF) and human GIP (PDB ID, 7CK6) show a high degree of structural homology despite low sequence homology (Wang *et al.*, 2020). Substrates for protein import are recognized by the receptor subunits Tom20, Tom22, and Tom70 (Dekker *et al.*, 1998; Meisinger *et al.*, 1999; Brix *et al.*, 2000). Precursor proteins with a N-terminal matrix-targeting sequence (mts) comprise up to two-thirds of the imported proteins (Morgenstern *et al.*, 2017; Wiedemann and Pfanner, 2017) and are recognized by Tom20 and Tom22 (Heijne, 1986; Shiota *et al.*, 2011). The receptor proteins then deliver the precursor proteins to the GIP, initiating their import through the central Tom40 gate (Meisinger *et al.*, 1999; Shiota *et al.*, 2015; Bausewein *et al.*, 2017). The association of Tom22 with the GIP-subunit Tom40 obviously is weaker than the association of Tom5, Tom6, and Tom7 with Tom40 (Dekker *et al.*, 1998), although Tom22 has multiple interaction points with Tom40 (Shiota *et al.*, 2011, 2015; Bausewein *et al.*, 2017; Sakaue *et al.*, 2019). Other studies found fractions of dimeric TOM-GIP without Tom22 (Sakaue *et al.*, 2019; Araiso *et al.*, 2020). The interaction of the surface receptors Tom20 and Tom70 with the GIP apparently is even weaker. Tom20 (and Tom70) was not found at the 400–440 kDa position of the separated GIP complex (Dekker *et al.*, 1998), and latest cryo-EM structures of monomers and dimers of the TOM complex contain no Tom20, only the trimeric TOM complex (Araiso *et al.*, 2020). While few putative Tom40–Tom20 interaction sites were found (Shiota *et al.*, 2015), a plethora of other proteins interacting with Tom20 are predicted (STRING-consortium, 2020). These data suggest that the receptor Tom20 might not be a permanent compound of the TOM complex but rather dynamically assembles and disassembles. We set out to test this dynamic model by determining the mobility of the receptor subunit Tom20 in the OMM in situ in mammalian cells. Previously, we found that at least two subpopulations of Tom20 with respect to lateral mobility exist (Appelhans *et al.*, 2012). That could represent freely diffusing Tom20 and Tom20 bound to the TOM. Here, we compared the mobility of fluorescent-labeled Tom20 with that of the GIP subunit Tom7. Following the model that only a fraction of Tom20 is bound to the GIP, we expected that the median mobility of Tom20 would be higher than the mobility of Tom7. Tom7 was chosen as a GIP subunit, since it was consistently found in all oligomeric TOM forms (Wang *et al.*, 2020). The spatiotemporal organization of Tom subunits Tom20 and Tom7 was determined by single particle tracking (SPT) of fluorescence labeled proteins (Appelhans *et al.*, 2017). Tom20 and Tom7 were successfully labeled via the self-labeling Halo7-Tag (HT) that was genetically fused to the N-terminus (Tom7), respectively C-Terminus (Tom20) of the proteins (Lisse *et al.*, 2011; Appelhans and Busch, 2017). After post-translational staining with HaloTag-Ligand (HTL) conjugated to fluorescent dyes, single fluorescent particles were localized and tracked as described before (Appelhans and Busch, 2017). We found that the median mobility of Tom20 was higher than that of Tom7. To obtain the diffusion constant of Tom20 associated with the GIP, Tom20 was then covalently ligated with Tom7 on the post-translational level by using the recently introduced ultrafast self-splicing split intein Gp41-1 system (Bhagawati *et al.*, 2020). The traceless split intein system allows ligation in situ and avoids the challenge of correct import and assembly of a genetically encoded Tom20-HT-Tom7 fusion protein. When Tom20 was spliced to Tom7, the mobility of Tom20 decreased, while Tom7 diffusion was unchanged, indicating successful cross-linking of Tom20 with the GIP. Finally, we studied Tom20 dynamics in the presence of high import substrate load. Under this condition, the mobility of Tom20 decreased significantly. Together, this study shows that the lateral dynamics of Tom20 in the OMM is flexible and substrate-dependent.

RESULTS

We here put for testing that the receptor subunit Tom20 is dynamically associated with the GIP. To test this hypothesis, we conducted SPT microscopy with fluorescence-labeled proteins and fluorescence lifetime imaging microscopy (FLIM).

Generation of Tom20 and Tom7 probes to study their assembly and spatiotemporal dynamics

For labeling of mammalian TOM complex subunits in HeLa cells, which are the cell models for our studies, fusion proteins of Tom20 and Tom7 with fluorescent proteins (FP) or the self-labeling HT were generated. Therefore, HT or FP was genetically fused to the receptor subunit Tom20 (Tom20-HT/FP) and the GIP subunit Tom7 (HT-FP-Tom7) (Supplemental Table S1). On average, Tom20 content was 2.6× in stably transfected Tom20-HT cells (Supplemental Figure S1). First, we checked the functionality of tagged Tom20 and Tom7. Therefore, yeast cells expressing Tom20-HT and HT-Tom7 were generated by homologous recombination in the genome (Supplemental Table S2). Tom20-HT and HT-Tom7 expressing cells were spotted as serial dilutions onto YPD or YPLactate and YPGlycerol plates, grown at 30°C and compared with deletion strains of the respective genes. The growth test shows that tagging Tom7 N-terminally or Tom20 C-terminally with the HT resulted in functional proteins (Supplemental Figure S2). To determine correct localization of Tom20-HT and Tom7-HT, cells expressing the respective construct were stained by supplying the HTL conjugated to a fluorescent dye. Since live cell imaging was conducted, cell-permeable HTL-dyes, HTL-tetramethyl rhodamine (TMR^{HTL}; λ_{exc} = 561 nm; λ_{em} > 570 nm), $JF646^{HTL}$ (λ_{exc} = 640 nm; λ_{em} > 650 nm), or HTL-silicon rhodamine (SiR^{HTL}; λ_{exc} = 640 nm; λ_{em} > 650 nm) were used (Lisse *et al.*, 2011). Tagged Tom20 and Tom7 showed clear mitochondrial localization in yeast (Supplemental Figure S2) and HeLa cells (Figure 1A).

Next, the assembly of Tom20-FP and FP-Tom7 into TOM complexes was checked. Therefore, stable HeLa cells expressing Tom20-EGFP and EGFP-Tom7 were generated. The assembly was tested by immunodetection after separation in a Blue Native (BN) PAGE. EGFP-Tom7 was found in a high molecular weight TOM / GIP complex assembly (~600 kDa, indicated as ***) that also contained Tom40 and Tom20 (Figure 1, B and C). We assign this high molecular weight complex to the trimeric active TOM complex (TOM_3), in accordance with previous reports on the size of the TOM holo complex with all subunits, which was estimated to be 490–600 kDa by gel filtration (Ahting *et al.*, 1999). In addition, we identified a complex of ~450 kDa with Tom7 and Tom40 (** in Figure 1, B and C). This complex was found in cells expressing Tom20-EGFP and EGFP-Tom7, but not in wild-type cells, suggesting that overexpression of TOM subunits, at least Tom7 and Tom20, promotes the formation of an intermediate state of assembly, where the complex itself does not contain Tom20. Such an intermediate complex was described before (Model *et al.*, 2002; Bykov *et al.*, 2020). Concerning the exact molecular weights, it has to be mentioned that the accuracy of molecular weight

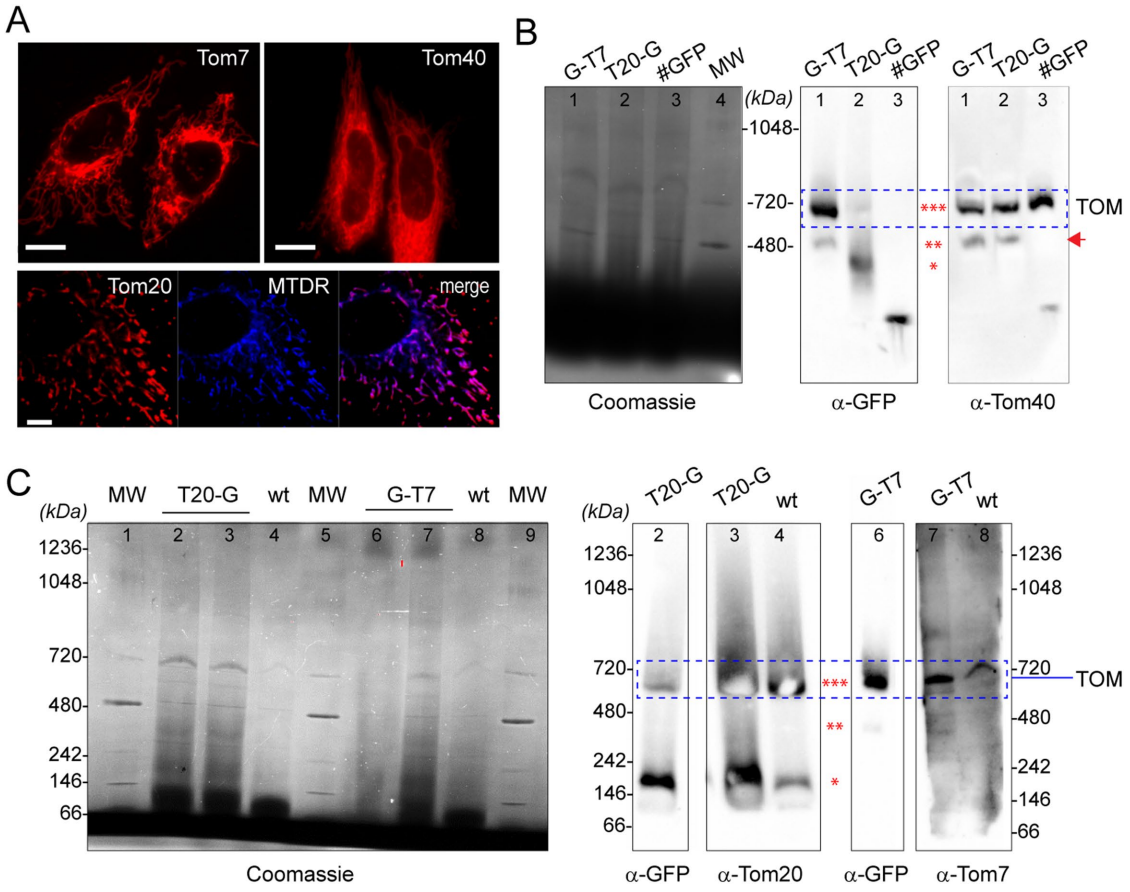

FIGURE 1: Localization and assembly of tagged TOM subunits in mitochondria. (A) Subcellular localization of Tom7 and Tom20 conjugated to the HT and stained with TMR^{HTL}. The HeLa cells expressing Tom20-HT (TMR^{HTL}, 30 nM; abs/em ~561/582 nm) were costained with MTDR (25 nM; abs/em ~644/665 nm). (B–D) Assembly of tagged TOM subunits into the TOM core complex. BN-PAGE, Coomassie-stained (left panels), and immunostaining of TOM subunits Tom40, Tom20, Tom7, and GFP in non-transfected cells (wt), cells expressing MPP-sEcGFP (#), Tom20-GFP (20#), and GFP-Tom7 (#7), respectively. Molecular weight marker: M. Scale bars: 5 µm (Tom7) and 10 µm (Tom20, MTDR, merge). ***Putative trimeric TOM, **putative dimeric TOM, *subcomplex with Tom20.

determination is limited by the presence of unknown amounts of detergents in these preparations and by the fact that, although membrane proteins are analyzed, the marker proteins are soluble (Rapaport, 2002). The intermediate complex (**) was not found in wild-type cells or cells overexpressing mitochondrial processing peptidase (MPP) fused to superecliptic green fluorescent protein (sEcGFP) resulting in MPP-sEcGFP (Figure 1B, arrowhead). Taking into account previous observations that Tom20 does not assemble to the dimeric TOM core complex but only to the trimeric complex (Araiso *et al.*, 2020) let us conclude that the 450-kDa TOM complex is the dimeric TOM_2. Apparently, TOM_2 is of intermediate nature (Model *et al.*, 2002; Rapaport, 2002; Araiso *et al.*, 2020). In addition to its presence in the trimeric active TOM_3 complex, Tom20 was found in complex of ~200 kDa (indicated as *) that did not contain Tom7 or Tom40. The complex shows a molecular weight a magnitude higher than Tom20, suggesting interaction with other proteins. Recently, it was shown that the receptor subunit Tom22 associates with porin (Sakaue *et al.*, 2019). We hypothesized that in analogy Tom20 might interact with the highly abundant voltage-dependent anion channel VDAC. Indeed, we found VDAC oligomers at the same position as Tom20 in BN-PAGE at a molecular weight of ~200 kDa (*) (Supplemental Figure S3), suggesting a possible VDAC–Tom20 interaction. Tom20–VDAC interactions have been proposed before (STRING-consortium, 2020). We conclude that a significant subpopulation of Tom20 is not associated with the active TOM complex but interacts with VDAC, simi-lar to how Tom22 interacts with porin in yeast (Sakaue *et al.*, 2019). Indeed, in cells overexpressing a labeled version of Tom20, the labeled version was found predominantly in the ~200-kDa complex, although expression of the labeled version did not generally interfere with assembly of Tom20 with the trimeric TOM (compare Figure 1, B and C, α-Tom20 lanes). Apparently, excess Tom20-tag is captured in the low-molecular complex. However, since tagging of endogeneousTom20 had no effect on mitochondrial shape and cell growth under respiratory conditions in yeast (Supplemental Figure S2) and overexpressing of Tom20-GFP in HeLa cell did not alter mitochondrial morphology we assume that function-ality is not hampered by Tom20-GFP overexpressinon.

In sum, we found that genetic fusion of Tom7 and Tom20 did not interfere with their assembly into the trimeric TOM core complex and function of the import machinery, that dimeric TOM does not contain Tom20, and that a substantial subpopulation of Tom20 is found in a complex that does not contain Tom7 and Tom40, but likely VDAC. This strongly suggests that Tom20 would in general display a different spatiotemporal behavior than TOM/Tom7 in situ.

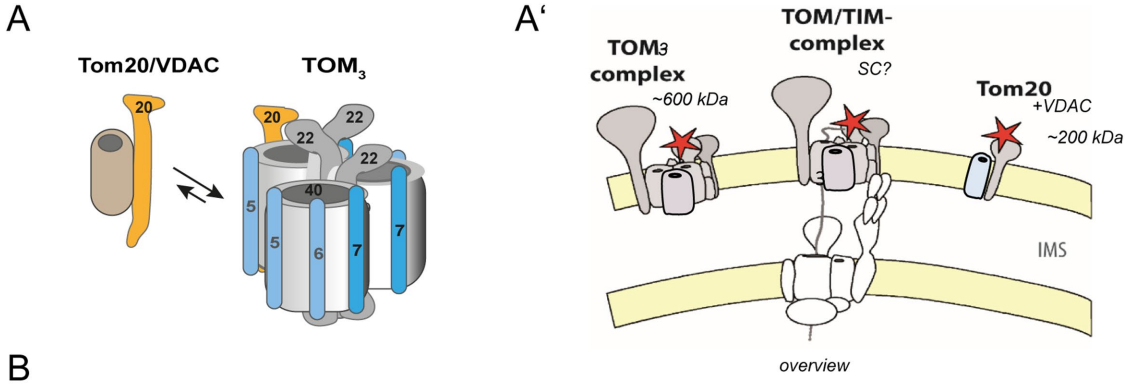

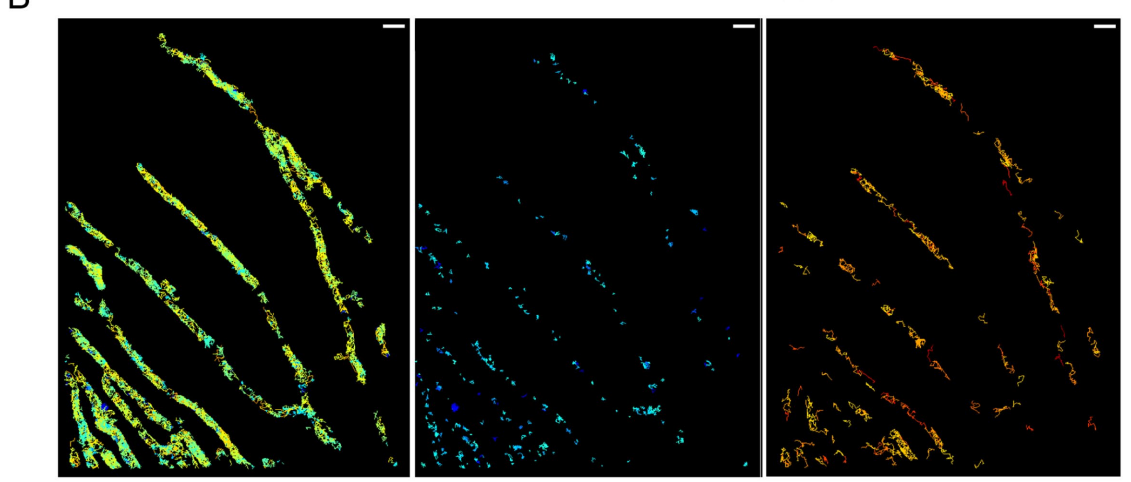

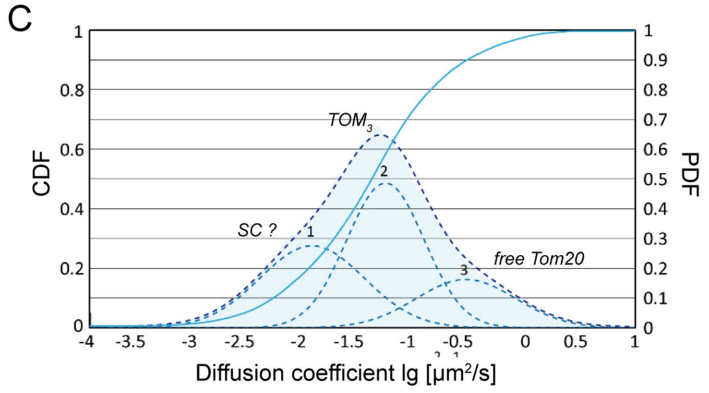

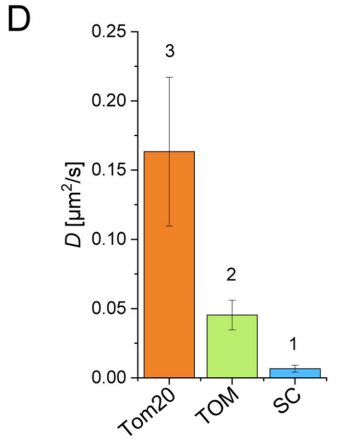

Tom20 Peak	lg(D) [lg(µm²/s)]	Diffusion Coefficient D [µm²/s]	Probability Density
1	-1.964	0.011	0.28
2	-1.288	0.052	0.49
3	-0.541	0.288	0.16

FIGURE 2: Identification of Tom20 subpopulations with different mobility in HeLa mitochondria. (A) Schematic model of subpopulations of Tom20 deduced from complex separation by BN-PAGE. TOM_3: trimeric TOM complex, Tom20/VDAC. (A') Schematic model of subpopulations of Tom20 deduced including formation of import supercomplexes with the translocase of the inner membrane (TIM). TOM_3: trimeric TOM complex, Tom20/VDAC, SC: supercomplex of TOM/TIM. (B) Trajectory maps of Tom20 (Tom20-HT/ TMR^{HTL}) in mitochondria in part of a living cell (~10 mitochondria are shown). Left panel: Trajectory map of all trajectories identified, cumulative image of all frames. Middle panel: Trajectories of the subpopulation with $D = 10^{-4}$ µm²/s to $D = 10^{-2}$ µm²/s; right panel: trajectories with $D = 10^{-0.75}$ and $D = 4 \times 10^{-1}$ µm²/s. Every trajectory is color-coded according to its diffusion coefficient. The color range was set from blue (low *D*) over green and yellow to red (high *D*). Recording: 33 Hz. Scale bars: 1 µm. (C) Determination of diffusion coefficients *D*. PDF and CDF for diffusion coefficients *D* of Tom20, plotted as –log *D*. Three subpopulations with different mean *D* were fitted. Table: –log *D*, *D* and weight of the three fitted fractions. Total number of trajectories analyzed: 172,212. (D) Plotting of diffusion coefficients *D* [µm²/s] for putative SC-Tom20 (#1; immobile; blue bar), Tom20/TOM_3 (#2, less mobile, green), and highly mobile Tom20 (#3; red) calculated from > 16 different cells ($N = 5$).

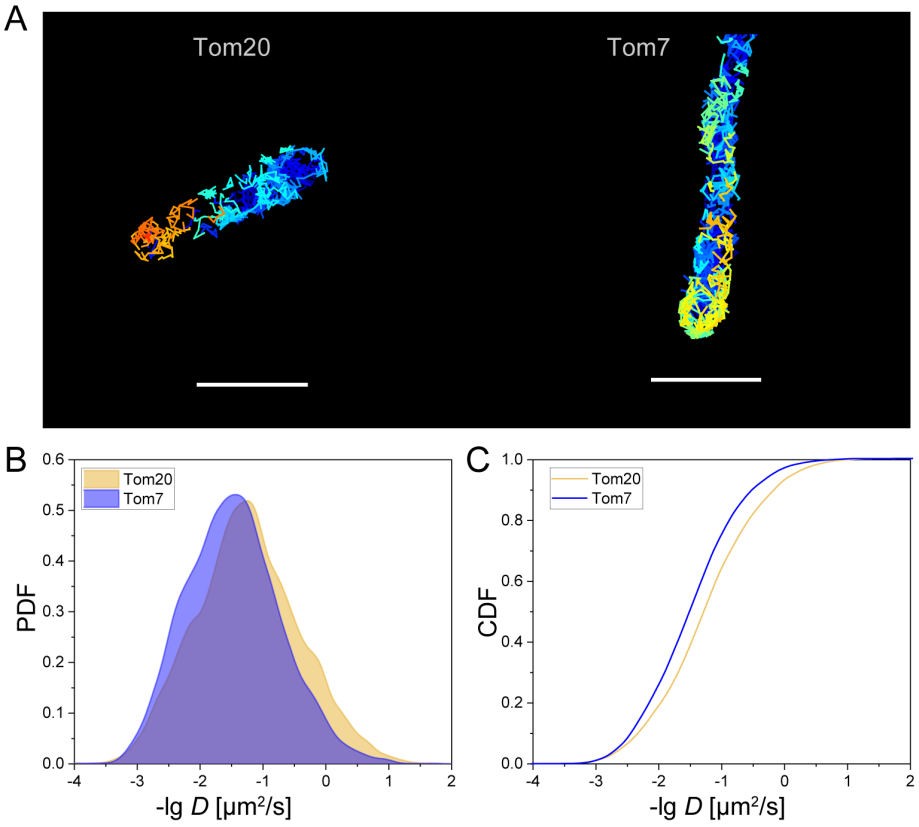

FIGURE 3: Determination of Tom20 and Tom7 diffusion in the OMM of mitochondria. (A) Trajectory maps of Tom20-HT/SiR^{HTL} and HT/SiR^{HTL}-Tom7 in individual mitochondria. Individual trajectories are color-coded according to their diffusion coefficient from cold (lower *D*) to hot (high *D*). (B) Distribution function of all diffusion coefficients of Tom20 and Tom7 as PDF, plotted as –log *D*. More than 11,000 trajectories from >5 videos were analyzed per condition (100 Hz, 2000 frames/video). (C) Corresponding CDFs of the diffusion coefficients. Scale bars: 1 µm (A).

Single molecule tracking displays subpopulations of Tom20 with different diffusion behaviors

We expected that 1) Tom20 on average would display a different mobility than Tom7, and that 2) subpopulations of Tom20 characterized by different diffusion behaviors would be found in living cells related to different Tom20/complexes (Figure 2A). According to the BN-PAGE immunostaining, a smaller complex (~200 kDa) and a larger complex (~600 kDa) with Tom20 exist. In addition, active translocating complex TOM_3 might form a supercomplex (SC) with translocase of the inner membrane (TIM) (Figure 2A'), the translocase of the inner mitochondrial membrane, that probably is disrupted during protein complex isolation and thus not found in immune-blots.

To test for differently dynamic Tom20 subpopulations, we determined the diffusion coefficients of the receptor subunit Tom20 by single particle tracking (SPT) as recently described (Appelhans *et al.*, 2012, 2018; Appelhans and Busch, 2017). To obtain diffusion coefficients *D*, the mobility of fluorescent Tom20-HT/SiR^{HTL} was recorded. For the generation of trajectories, localizations of the same emitter in subsequent frames were linked using a tracking algorithm developed by the Danuser lab (Jaqaman *et al.*, 2008). Figure 2B shows a trajectory map of all tracked Tom20 in several long tubular mitochondria imaged in part of a live HeLa cell. Single trajectories are depicted in a heat color map according to the respective diffusion coefficient *D*: a cold color indicates small *D*; a hot color indicates higher *D* values. The map shows an equal distribution of hot and cold trajectories across individual mitochondria (homogenous color distribution), suggesting that subpopulations of Tom20 molecules characterized by different mobility are not spatially separated in different parts of mitochondria. Next, from the total pool, only the immobile molecules ($D < 0.010$ µm^2/s, Figure 2B, middle panel) are shown, or in a second window, only the fast molecules with diffusion coefficients between $D = 10^{-0.75}$ µm^2/s and $D = 10^{1}$ µm^2/s (right panel). Then, a histogram of all diffusion coefficients *D* obtained from single trajectories was generated. From this, either the median diffusion coefficient D_{median} or the diffusion coefficient *D* for different subpopulations was extracted by fitting the probability density function (PDF) of the –log *D* plot (Figure 2C). We found tree fractions characterized by different diffusion coefficients *D*. These fractions were assigned to the different states of Tom20. Likewise, the Tom20 fraction with highest mobility was assigned to free Tom20, the fraction with intermediate *D* to Tom20 associated with the TOM complex and the immobile fraction to a putative TOM/TIM SC. Thus, the diffusion data support the existence of different Tom20 subpopulations in the membrane.

Tom20 shows a higher mobility than the GIP subunit Tom7

Next, we compared the mobilities of Tom20 and Tom7 in the mitochondrial outer membrane in situ. We assumed a lower mobility for Tom7 as an integral part of the TOM complexes TOM_2 and TOM_3. Comparison of the trajectory maps of Tom20 and Tom7 displays no significant difference in the course of the trajectories, but higher *D* values were found for Tom20 than for Tom7 (as indicated by the color codes in red and orange in Figure 3A). Ensuing, diffusion coefficients for single trajectories were plotted as PDF histograms. Although the PDF histograms show an overlap, it also becomes clear that Tom20 has a population with higher mobility than Tom7 (Figure 3B). The cumulative density function (CDF) of the *D* values shows a shift toward lower *D* values for Tom7, too (Figure 3C). In step length histograms, Tom20 displays larger step sizes than Tom7 (Supplemental Figure S4). The higher mobility of Tom20 in comparison to Tom7 is in line with the observation that a subpopulation of Tom20 is not associated with the trimeric TOM complex, unlike Tom7, which is always associated with TOM (Figure 1).

Ligation of Tom20 and Tom7 proteins by ultrafast split Gp41-1 intein

Next, we attempted to induce an increase in the association of Tom20 with the TOM complex to test whether this would affect the mobility of Tom20. We expected that increasing Tom20/TOM association would decrease Tom20 mobility, as TOM is likely to be more mobility restricted, as shown by the Tom7 diffusion data shown in Figure 3 and suggested earlier (Kuzmenko *et al.*, 2011). Due to the available N-terminus of Tom7 in the cytosol, a ligation of the

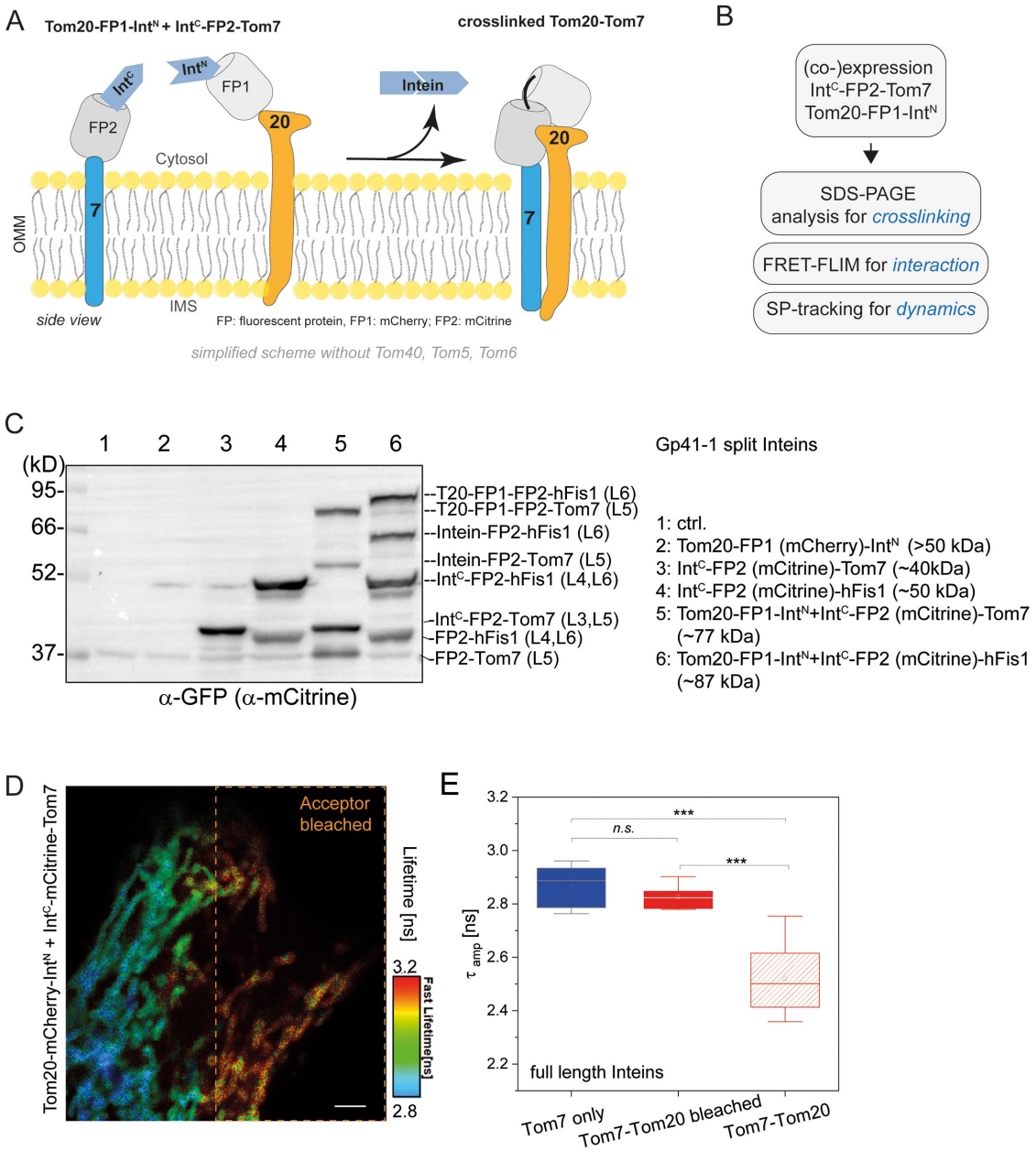

FIGURE 4: Cross-linking of Tom20 to Tom7 via split inteins increases Tom20–Tom7 interaction. (A) Reaction of split inteins Tom20-FP1-Int^N and the Int^C-FP2-Tom7. Successful splicing will result into ligation of Tom20-FP1 to the GIP protein FP2-Tom7. FP1: FP 1 (mCherry) and FP2: FP 2 (EGFP). For simplification, only Tom7 and Tom20 are shown. (B) Workflow to determine cross-linking, interaction, and dynamics of Tom20 in relation to Tom7 before and after cross-linking. (C) Immuno-detection of SDS–PAGE-separated fusion proteins in cells expressing only Tom20-mCherry-Int^N (T20-FP1-Int^N), only Int^C-mCitrine-Tom7 (Int^C-FP2-T7), only Int^C-mCitrine-hFis1 (IntC-FP2-hFis1), and cells coexpressing Tom20-mCherry-Int^N and Int^C-mCitrine-Tom7 or Tom20-mCherry-Int^N and Int^C-mCitrine-hFis with a polyclonal anti-GFP antibody. (D) FRET/FLIM to monitor Tom20–Tom7 interaction. The image shows the mCitrine-Tom7 lifetime (color-coded) of a cell transfected with Gp41-1Int^C-mCitrine-Tom7 (donor) and Tom20-mCherry-Gp41-1Int^N (acceptor). mCherry was bleached in the region bounded by the dotted yellow rectangle. In the acceptor-bleached region, the had lifetime increased (see color-code). (E) Lifetimes τ_{amp} obtained after fitting the TCSPC histogram of mCitrine-Tom7 with a biexponential tail fit. τ_{amp} is composed of weighted lifetimes τ_1 and τ_2. Data from FLIM analysis of cells either transfected with donor mCitrine-Tom7 only (blue box), or with both donor and acceptor. For the analysis, six cells each were analyzed for the donor-only transfection conditions, while 12 cells (two transfections, six cells each) were analyzed for the double-transfection condition. Statistics: Anova; $p \leq 0.001$, ***$p \leq 0.01$, **$p \leq 0.05$, *n.s., non-significant. Scale bars: 2 μm (D).

cytosolic C-terminus of Tom20 to Tom7 seemed feasible. However, a genetic fusion of Tom20-HT-Tom7 likely would mess up with import, correct folding, and assembly of the construct. We therefore searched for an alternative to ligate Tom20 and Tom7. Gp41-1 split intein pairs enable such a proceeding (Volkmann and Mootz, 2013). Split inteins consist of two fragments, the Int^N and the Int^C fragments.

As soon as the fragments come into contact, the process of protein trans-splicing (PTS) is started in which first a folded intein domain is formed reconstituted and which cuts itself out of the precursor proteins, thereby covalently ligating the fused sequences (Volkmann and Mootz, 2013). Since the process requires folding of the of the intein domain, it is also a quality control step for correct import of the fusion proteins into the OMM. The Gp41-1 split intein is the fastest split intein with PTS occurring within a few seconds and a nanomolar affinity between the intein fragments (Carvajal-Vallejos *et al.*, 2012; Bhagawati *et al.*, 2020). We genetically generated Tom20-FP1-Int^N and Int^C-FP2-Tom7 with FP1 and FP2 as different FPs. After trans-splicing and release of the intein into the cytosol, the TOM subunits Tom20 and Tom7 are ligated as schematically depicted in Figure 4A. Ensuing, the formation of the splice product Tom20-FP1-FP2-Tom7 was analyzed by immunoblotting; the interaction of Tom20 and Tom7 by FLIM in combination with Förster resonance energy transfer (FRET) and the dynamics of the spliced Tom20–Tom7 was determined by SPT as outlined in Figure 4B.

Coexpressed fusion proteins that carried the Int^N and Int^C-peptide became successfully cross-linked, as the analysis of protein-gel shows (Figure 4C). The efficiency was ~30%. In protein extracts from cells coexpressing Tom20-mCherry-Int^N and Int^C-mCitrine-Tom7, additional bands of higher molecular weight appeared, indicating the formation of Tom20-mCherry-mCitrine-Tom7 (FP1: mCherry; FP2: mCitrine). As by-products, Tom20-FP1 and FP2-Tom7 were also found in the coexpression assay; obviously the trans-splicing removed the intein but did not cross-link the proteins of interest. The coexpression of Tom20-meGFP-Int^N and Int^C-HT/TMR^{HTL}-Tom7 had no severe effect on mitochondrial morphology (Supplemental Figure S5). In an additional experiment, Tom20-mCherry-Int^N and Int^C-mCitrine-hFis were coexpressed to check efficiency of the intein system. hFis is the human mitochondrial fission protein and also localized in the OMM (Yu *et al.*, 2005), but to our knowledge has no interaction with Tom20. Likewise, this self-splicing reaction resulted in a Tom20-mCherry-mCitrine-hFis product (Tom20-FP1-FP2-hFis) (Figure 4C). Thus, the ultrafast Gp41-1 split intein system was successful in the ligation of Int^C- and Int^N-tagged proteins. Roughly, ~30% of Tom20-FP1 were spliced to FP2-Tom7 and ~50% to FP2-hFis. For the cross-linking of Tom20-mCherry-Int^N and Int^C-mCitrine-hFis, we suggest that the driving force for reaction was the high affinity between the split inteins (K_D = 9.2 ± 1.3 nM) (Bhagawati *et al.*, 2020), since no interaction between the proteins is expected (STRING-consortium, 2020). However, we cannot conclusively say which was the driving force for the formation of the Tom20–Tom7 cross-linking product, since k_{on}/k_{off} rates for the interaction between Tom20 and the GIP or Tom7 are unknown.

Coexpression and cross-linking of Tom20 and Tom 7 result in increased physical Tom20–Tom7 interaction

We next tested the interaction between Tom20 and Tom7 by means of FRET/FLIM using FPs. For interaction analysis, we compared the fluorescence lifetimes (τ) of donor constructs in the presence and absence of acceptors. τ was determined by analyzing time-correlated single photon counting (TCSPC) histograms. The decay curves were fitted with a tailored biexponential fit. For more details concerning fluorescence lifetime imaging, see our previous study (Sohnel *et al.*, 2016). For practical reasons, mCitrine fused to Tom7 (Int^C-mCitrine-Tom7) was used as a donor when testing full-length inteins. The energy acceptor was mCherry fused to Tom20 (Tom20-mCherry-Int^N).

First, we investigated the effect of the splicing of Tom20 and Tom7 by the fully active and high-affinity Gp41-1 split intein. Cells coexpressing donor and acceptor constructs were mounted under a fluorescence microscope with a TCSPC module. After taking one regular image, the acceptor was bleached in half of the field of view. That allows for direct comparison of the donor lifetime in the presence and absence of the acceptor in single cells (Figure 4D). The blue box shows the lifetime of mCitrine-Tom7 in single transfected cells (Figure 4E). Next, we compared the lifetime of mCitrine in cells coexpressing Int^C-mCitrine-Tom7 and Tom20-mCherry-Int^N. The lifetime of mCitrine was significantly reduced (red-shaded box; $p \leq 0.001$). Bleaching of the acceptor mCherry (regions bounded by yellow dotted lines in Figure 4D) led to a significant increase of the mCitrine lifetime (red box in Figure 4E) resulting in a τ similar as the lifetime of samples where no acceptor was present (Tom7 only; blue box). The result indicates that Tom7 was interacting with Tom20 in the coexpressing samples.

Splicing of Tom20 to Tom7 reduces the mobility of Tom20

Next, we asked whether post-translational ligation of Tom20 to Tom7/TOM would affect the mobility of Tom20. According to our model, Tom20 associated with the TOM_3 should have lower mobility. Thus, if more Tom20 is ligated with the TOM, its mobility should be reduced. We again performed SPT of Tom20 in a cell line in which Tom20-HT-Int^N was expressed in combination with Int^C-mCitrine-Tom7. According to the SDS-immune blotting and the FRET/FLIM results, the coexpression resulted in the splice product Tom20-HT-mCitrine-Tom7 after release of intein. Trajectory maps of Tom20, respectively, Tom20–Tom7 were generated by overlaying all trajectories (Supplemental Figure S6). For every trajectory, the diffusion coefficient was determined. Finally, all diffusion coefficients obtained for the different settings (Tom20-FP-Int^N, Tom20-HT-Int^N + Int^C-mCitrine-Tom7, Int^C-HT-Tom7) were compared. From the individual trajectories relevant data as median diffusion coefficients, the lifetime of trajectories, the precision of localization, and signal-to-noise ratios were determined (Figure 5; Supplemental Figure S7). The overlay of the diffusion coefficient's PDFs and CDFs show a shift of the diffusion coefficients of ligated Tom20–Tom7 toward lower *D* (Figure 5B).

High load of import substrate substantially decreases the mobility of the receptor Tom20

Thereupon we tested the effect of high substrate levels for Tom20 on its mobility. We generated a mitochondria-targeted GFP variant by fusing sEcGFP to C-terminus of the MPP subunit β (MPP60). The mts of MPP60 has a binding motive typical for Tom20 with an amphiphilic helix, eight basic and two acidic residues (Claros and Vincens, 1996). MPP-sEcGFP was localized to mitochondria (Supplemental Figure S8) and mitochondrial preparations contained a protein band of ~71 kDa size, which is the molecular weight of MPP-sEcGFP (Figure 1B, #). A strong promotor (CMV) was used and a stable cell was generated that constitutively expressed MPP-sEcGFP. The trajectory map of Tom20-HT/SiR^{HTL} in mitochondria of MPP–sEcGFP-expressing cells is shown in Figure 5A. Information about signal to noise, localization precision, and mean trajectory lifetime and a comparison of slow and fast diffusing particles are found in the Supplemental Material (Supplemental Figure S9). The PDF and CDF of the diffusion coefficient distribution shows a clear overall reduction of mobility when compared with the mobility of Tom20. The underlying peak of highly mobile Tom20 (free Tom20) was reduced. Instead, the slow population on the flank with low diffusion coefficients became larger. This could be Tom20 in an active translocating TOM3/TIM SC.

We also determined the mean-square displacements (MSDs) of Tom20, Tom7, Tom20–Tom7, and Tom20 plus substrate. In the

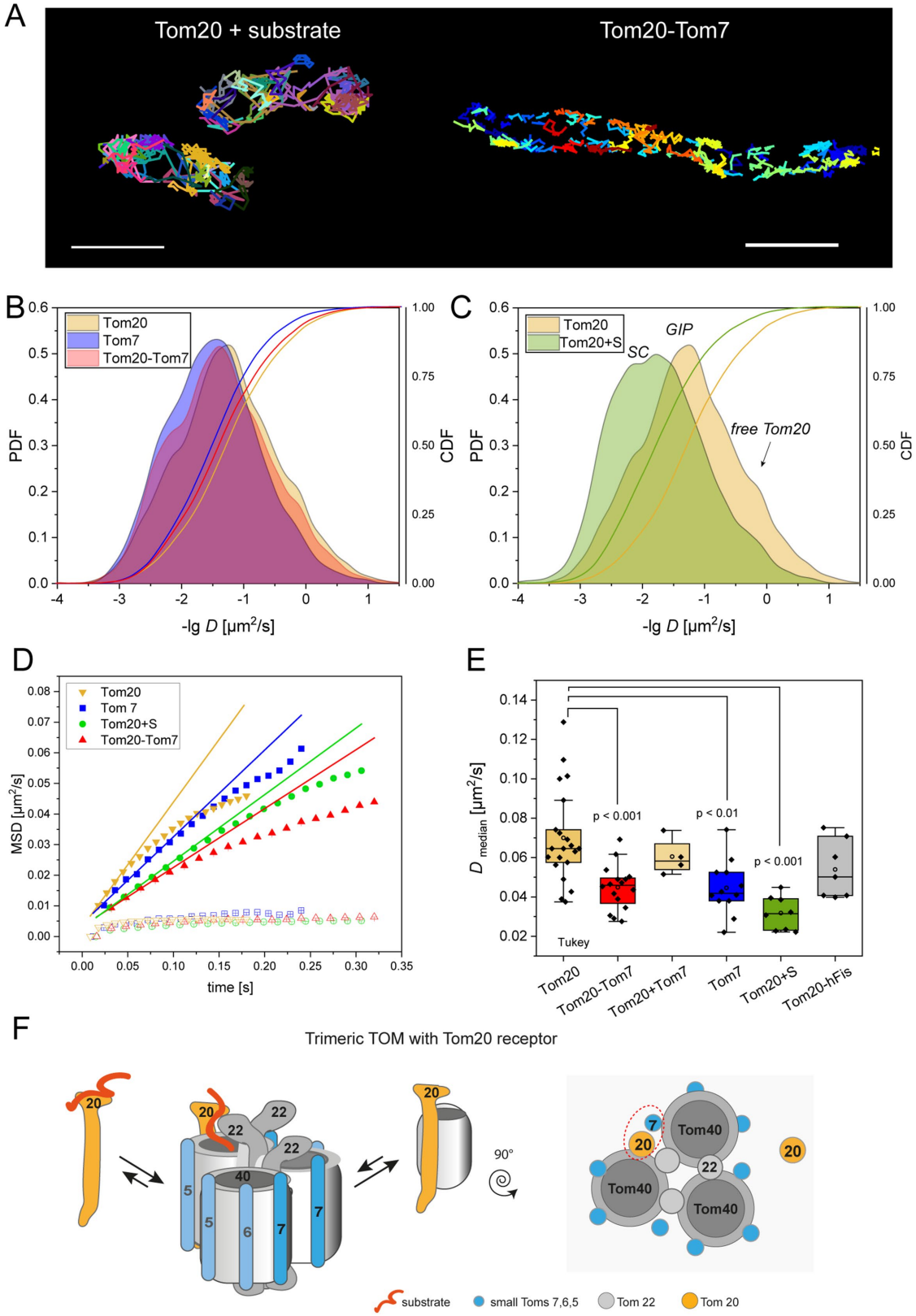

FIGURE 5: Substrate binding and artificial cross-linking of Tom20 to TOM via Tom7 reduces its mobility. (A) Trajectory maps of Tom20- HT/SiR^{HTL} in cells with high substrate load for mitochondrial import and of Tom20-HT/SiR^{HTL}-Tom7 in two mitochondria. Individual trajectories were color-coded according to their appearance. Scale bars: 1 µm. (B) Probability density function diagram (PDF) and CDF for diffusion coefficients of Tom20, Tom7, and Tom20–Tom7 plotted as –log *D*. More than 11,000 trajectories were analyzed (recording 2000 frames with 100 Hz per video, >5 videos analyzed per condition). (C) PDF and CDF diagram for diffusion coefficients of Tom20 and Tom20 plus substrate (Tom20 + S) plotted as –log *D*. More than 18,000 trajectories were analyzed (recording 2000 frames with 56 Hz per video,

short time range (30–75 ms), Tom20 displayed the highest MSD. Tom20–Tom7 and Tom20 plus substrate showed similar MSD values. Their MSDs were significantly lower than those of Tom7 or Tom20 (Figure 5D).

When we compared the median diffusion coefficients obtained from the cumulative probability density (Figure 5E; Supplemental Figure S10), the mobility of Tom7 (D_{Tom7} = 0.045 μm²/s, SD ± 0.013 μm²/s) was significantly lower than that of Tom20 (D_{Tom20} = 0.070 μm²/s; SD ± 0.023 μm²/s, $p < 0.01$). A similar diffusion coefficient (D = 0.088 μm²/s) was found by SPT with Tom20-fSNAP (Kondadi *et al.*, 2020). When Tom20 was cross-linked to Tom7 via the self-splicing intein, the mobility of the resulting Tom20–Tom7 product ($D_{Tom20–Tom7}$ = 0.045 μm²/s, SD ± 0.011 μm²/s, $p < 0.001$) was similar to the Tom7 mobility (D_{Tom7} = 0.045 μm²/s, SD ± 0.013 μm²/s, $p < 0.01$) in line with a successful ligation to the TOM complex. The decrease in mobility was not caused by the presence of higher Tom7 levels, as coexpressed Tom20 (without split inteins) maintained its higher mobility ($D_{Tom20+Tom7}$ = 0.060 μm²/s, SD ± 0.009 μm²/s). Also, trans-splicing of Tom20 to hFis had no effect on the mobility of Tom20. Most importantly, the presence of high substrate load (Tom20 + S) reduced the median diffusion coefficient of Tom20 to the half ($D_{Tom20+S}$ = 0.032 μm²/s; SD ± 0.008 μm²/s; $p < 0.001$) (Supplemental Tables S4A and S4B).

Together, these results substantiate the model that under normal conditions, a significant fraction of Tom20 is not associated with the TOM_3. When the import substrate load rises, more Tom20 associates with the active TOM_3, which results in overall decreased mobility (Figure 5F). The slowest fraction could be the active TOM_3/TIM, a quasi-immobile supercomplex that is spanning two membranes and not easy to be found in native preparations.

CONCLUSION

Here, we quantified the spatiotemporal behavior of the preprotein receptor Tom20 to determine its association with the general mitochondrial import pore, GIP. The GIP was found to be mainly a trimeric TOM complex. As we show, Tom20 is part of the trimeric TOM complex. An intermediate stage of lower molecular weight, possibly a dimeric TOM complex, did not contain Tom20. In addition, Tom20 was found in a complex with a size of ~200 kDa. This complex likely represents an association with VDAC and did not contain Tom40 or Tom7. Tom40 and Tom7 were found exclusively in the dimeric and trimeric TOM complexes. Single particle tracking showed that Tom20 was generally more mobile than Tom7. When Tom20 was exposed to higher substrate amounts, its mobility decreased significantly and became similar to that of Tom7. Physical ligation of Tom20 with Tom7 via intein-mediated protein trans-splicing also resulted in decreased mobility of the Tom20–Tom7 fusion construct, likely due to its tight association with the TOM via Tom7. FRET/FLIM analyses showed a decrease in the fluorescence lifetime of labeled Tom20 but not of Tom7 after trans-splicing to Tom7, demonstrating that Tom7 is primarily associated with the TOM complex but that Tom20 is not. Overall, we have shown here for the first time by superresolution imaging that Tom20 is dynamically associated with the active translocating TOM_3 but not with the TOM_2 complex. It is likely that this association with TOM_3 is due to the substrate-delivering activity of Tom20 which induces an association. In the free state, Tom20 is likely associated with VDAC. This spatiotemporal behavior of Tom20 is similar to that recently reported for Tom22 in yeast, where one subpopulation of Tom22 interacts with porin and another subpopulation associates with the trimeric TOM (Sakaue *et al.*, 2019). Our data provide further evidence for the model that the trimeric rather than the dimeric TOM complex is the active translocase (Araiso *et al.*, 2020) and that Tom20 is dynamically linked to the TOM complex.

MATERIALS AND METHODS

Request a protocol through *Bio-protocol*.

Cell culture

HeLa WT and stably transfected Tom20-HT expressing cells were cultivated in MEM Earle's Salt (5.6 mM glucose + L-glutamine) supplemented with 10% fetal calf serum, 1% HEPES, and 1% nonessential amino acids at 37°C and 5% CO_2. The cells were split when they were 80–100% confluent using Trypsin/EDTA for cell detachment. HeLa cells were purchased from the Leibniz Institute DSMZ-German Collection of Microorganisms and Cell Cultures and transiently transfected by the calcium transfection method if required (HT-Tom7, HT-Tom40). The transfected cells were used 48–72 h after transfection.

Confocal imaging

Cells grown on glass coverslips were incubated in medium with TMR^{HTL} (30 nM) and MitoTracker Deep Red (MTDR) (25 nM) for 30 min. After 30 min, cells were washed once with phosphate-buffered saline and once with medium. Fluorescence was recorded with a cLSM [Leica SP8, equipped with a white light laser (WLL)], a 63× water objective, numerical aperture (N.A.), and special hybrid GAsP detectors. Images were recorded sequentially for TMR and MTDR signals (line scanning mode). Cells were kept at 37°C and 5% CO_2 during the measurement. TMR was excited with the laser line 561 nm (WLL) and emission was recorded between 550 and 620 nm; $\lambda_{abs/em}$ were 644/665 nm for MTDR.

Split inteins

This project used split inteins to covalently link two target proteins presented on the OMM in order to control their interactions and localization dynamics. Split inteins are autocatalytic proteins that can ligate their flanking protein sequences (exteins) via a native peptide bond and in the process excise themselves out of the original precursor proteins.

In this project, we used an ultrafast split intein called the Gp41-1 intein (Carvajal-Vallejos *et al.*, 2012). In all the following descriptions, Int^N and Int^C refer to the N- and C-terminal fragments of the Gp41-1 intein, including five residues on the N-terminus of the Int^N and five residues on the C-terminus of the Int^C, which are derived from the original context of the intein. HeLa cells were transfected with the Int^N

>10 videos analyzed per condition). (D) MSD diagram showing MSDs of mobile and immobile molecules (open boxes). The first 30–75 ms were fitted with a linear fit. (E) Median diffusion coefficients D of Tom20, Tom7, and Tom20–Tom7 (Tom20-HT/SiR^{HTL}-mCitrine-Tom7) as well as of Tom20-HT/SiR^{HTL} in the presence of mCitrine-Tom7 and Tom20 in the presence of high substrate load. Also shown is the median D for ligated Tom20-hFis. $N \geq 2$ biological replicates. For detailed information, see Supplemental Table S3 and Supplemental Figures S5–S7. (F) Model for the association of Tom20 in the substrate bound state to the trimeric TOM complex. Left side: side view, right side: top view. The dotted ellipse indicates Tom20–Tom7 interaction, respectively cross-linking via Intein-splitting.

and Int^{C} fusion proteins: IntN-mCherry-Tom20 (*a*), Tom7-mCitrine-IntC (*b*), and hFis-mCitrine-IntC (*c*). HeLa cells were transfected with either constructs *a*+*b* or *a*+*c*. For FRET measurements, mCitrine was the donor and mCherry was the acceptor. Cells were also transfected with only *b* or *c* as donor-only controls. The fusion proteins Tom20 and Tom7 were in addition fused to the HT (Supplemental Table S1), when appropriate. The HT was labeled with TMR^{HTL}.

SDS and immunoblotting

Briefly, cell lysates from samples of confluent T-25 flasks (1 flask would last for 10–15 gels) were heated for 5 min (95°C); 20 µg of denatured proteins were then resolved by SDS–PAGE using self-casted 4–12% tricine-bis-acrylmaide gels (Bio-Rad). Gel contents were electro-transferred to polyvinylidene fluoride (PVDF) membranes (Millipore) using a semidry TransferApparatus (Trans-Blot SD; Bio-Rad). Equal loading was evaluated by Ponceau S staining. Membranes were blocked with 10% nonfat dry milk in TBS-T (200 mM Tris, 1.37 M NaCl, +0.1% Tween20) for 1 h. Membranes were incubated with primary antibodies overnight at 4°C. GFP was detected with polyclonal anti-GFP antibody (AB10145) purchased from Merck Millipore. After washes in TBS-T, detection was performed with HRP–conjugated secondary antibodies (1:2000). Membranes were washed in TBST and developed using standard chemiluminescence with ECL (SuperSignal WestPico Thermo Fisher) and imaged by ChemiDoc (Bio-Rad).

BN page electrophoresis and immunoblotting

For blue native (BN-)PAGE, cell lysates from two confluent T175 flasks were processed as described recently (Salewskij *et al*., 2020). In short, harvested cells were lysed, and mitochondria were enriched by differential centrifugation and solubilized via Digitonin ~50% (TLC) (Sigma-Aldrich, #D5628) 6 g/g mitochondria (Acin-Perez *et al*., 2008). The TOM complex was separated by means of high resolution BN electrophoresis as described in Wittig *et al.* (2007). First, the concentration of crude mitochondria was determined via the Bradford method using bovine serum albumin as a standard. For BN-PAGE analysis, 50 µg protein per pocket were loaded and separated via the vertical native gel 3–12% SERVAGel (Serva, #43251.01). In addition, a NativeMark Unstained Protein Standard (Thermo Fisher, #LC0725) was used for molecular weight estimation. However, it should be taken into consideration, in gradient gels, that native membrane protein behaves slightly different than free protein standard, especially in the high molecular weight range. Cathode and anode buffers were prepared as described in Wittig *et al.* (2006).

After separation, the proteins were electroblotted using the Mini-Vertical Blotting System (Expedeon, #EBX-700) onto Hybond-P- PVDF membranes (GE Healthcare). In blotting buffer (25 mM Tris, 192 mM glycin, 0,05% SDS, 20% methanol), protein transfer was performed overnight at 20 V and 4°C.

For immunodetection, the primary antibodies against GFP (Merk, #AB10145), Tom20 (Proteintech, #11802-1-AP), Tom7 (Proteintech, #15071-1-AP), and Tom40 (Santa Cruz, #sc-365467), and the secondary antibody Peroxidase AffiniPure Goat Anti-Mouse IgG + IgM (H+L) (111-035-068) or Goat anti-Rabbit IgG (H+L) (111-035-045) from Jackson ImmunoReasearch were used. The signal was detected using the Odyssey Infrared Imaging System (Li-COR Bioscience). The mean density of the detected bands was determined using the analysis tool measure of ImageJ after background subtraction.

SPT microscopy

Single particle tracking (SPT) was conducted with HT membrane proteins as described before (Appelhans *et al*., 2012, 2017; Appelhans and Busch, 2017). Living cells expressing HT subunits were imaged after the HT subunits were substoichiometrically labeled with SiR-HTL, a kind gift from Kai Johnson (SiR^{HTL}). For Tom20 tracking, a stably transfected Tom20-HT cell line was used. For HT-Tom7, the recording was performed 24 h after transient transfection. Before imaging, cells were incubated with 0.5–1 nM SiR^{HTL} for 30 min and then washed 3× with medium containing no phenol red; 0.5–1 nM were optimized concentrations taking into account the reaction rate constant for TMR^{HTL} that was determined before as 1×10^{6} $M^{-1}s^{-1}$ (Lisse *et al*., 2011). Images were recorded in medium without phenol red. Single molecule recording was performed with a microscope equipped with a total internal reflection fluorescence (TIRF) condenser and with an apochromatic 150× oil immersion objective designed for TIRF microscopy (150× TIRF objective, N.A. 1.45, Olympus, UAPO). TMR was excited with a diode-pumped solid-state laser (excitation 561 nm, 200 mW, Cobolt Jive 561) and the incident angle was set to achieve a highly inclined optical light sheet (Appelhans *et al*., 2012; Tokunaga *et al*., 2008). Usually, 1500–3000 frames were recorded (100, 63 Hz) with a back-illuminated electron multiplying charge-coupled device camera (Andor iXON 897, pixel size 16 µm^2). For comparison of the mobility of different subunits, videos were recorded with the same frame rate.

Analysis of SPTM-data

The analysis is described in (Appelhans and Busch (2017). Signals for single emitters were fitted with a 2D-Gaussian fit using the experimentally determined point spread function to calculate the center of the emission and the localization precision. Localizations of the same emitter in subsequent frames were linked using a tracking algorithm developed by the Danuser lab (Jaqaman *et al*., 2008). First, Tom7-HT/TMR^{HTL} was tracked; 3000 frames were recorded with frame rates of 33 and 56 Hz, respectively. To obtain diffusion coefficients, a histogram of the diffusion constants obtained from single trajectories was generated. From this, different subpopulations were extracted by fitting the probability density function of the log plot (Figure 1). In addition, MSDs were calculated with a sliding window of 5 steps.

FRET/FLIM

The procedure of FLIM is described in (Sohnel *et al*. (2016). Time-resolved fluorescence measurements were performed using a confocal laser scanning microscope (FluoView FV1000, Olympus) equipped with a TCSPC extension module (PicoQuant GmbH). The excitation source was a pulsed LDH-D-C-485 laser (PicoQuant GmbH) operated at a repetition time rate of 40 MHz. The output pulses were coupled into an optical fiber. The output at the fiber end was reflected from a beam splitter onto the base of a multiwell plate (Ibidi, 30 µl) or a glass coverslip via a 60× oil-immersion objective (UPLSAPO oil, NA 1.35, N/0.17/FN26.5, Olympus) upgraded with an objective heater (Bioptechs). For photon detection, a single photon avalanche diode was used. The acquisition was performed until at least 1000 photons in the brightest pixel were reached. To obtain the fluorescence lifetime of mCitrine, data analysis was performed with SymphoTime software (64 bit) and a biexponential tail fit with χ^2 minimization. The resulting values for the fluorescence lifetime were displayed on a standard false-color scale. The dwell time was 2 µs per pixel.

ACKNOWLEDGMENTS

We thank Bettina Rieger for valuable discussions and preliminary results on CN-PAGE and FRET/FLIM, Frances Hager for acquiring

first data on Tom20 dynamics, and Patrick Duwe for SDS–PAGE analysis and Christian Richter for writing the software for single particle analysis. Furthermore, we thank Nikolaus Pfanner and Thomas Rudel for inspiring discussions. The SiR^{HTL} substrate was a kind gift of Kai Johnson. We are thankful to Doron Rapaport for providing yeast strains. This research was funded by the DFG (Cluster-of-excellenceEXC1003 "Cells in Motion," FF project 2017-07 to K.B.B. and H.D.M. and the CRC944, INST190/167-2 and the z-project). M.B. acknowledges a postdoctoral fellowship from the Alexander von Humboldt Foundation, and A.G.M. is a recipient of an EMBO Advanced Long Term Fellowship (ALTF 609-2018).

REFERENCES

Acin-Perez R, Fernandez-Silva P, Peleato ML, Perez-Martos A, Enriquez JA (2008). Respiratory active mitochondrial supercomplexes. Mol Cell 32, 529–539.

Ahting U, Thun C, Hegerl R, Typke D, Nargang FE, Neupert W, Nussberger S (1999). The TOM core complex: the general protein import pore of the outer membrane of mitochondria. J Cell Biol 147, 959–968.

Appelhans T, Beinlich FR, Richter CP, Kurre R, Busch KB (2018). Multi-color localization microscopy of single membrane proteins in organelles of live mammalian cells. JoVE, e57690–e57690.

Appelhans T, Busch K (2017). Single molecule tracking and localization of mitochondrial protein complexes in live cells. Methods Mol Biol 1567, 273–291.

Appelhans T, Richter CP, Wilkens V, Hess ST, Piehler J, Busch KB (2012). Nanoscale organization of mitochondrial microcompartments revealed by combining tracking and localization microscopy. Nano Lett 12, 610–616.

Appelhans T, Wilkens V, Rieger B, Perkins G, Busch K (2017). Tracking and localization microscopy of single mitochondrial proteins in living cells. In: European biophysics journal with biophysics letters, New York: Springer, pp. S366–S366.

Araiso Y, Imai K, Endo T (2020). Structural snapshot of the mitochondrial protein import gate. FEBS J, *in press*.

Bausewein T, Mills DJ, Langer JD, Nitschke B, Nussberger S, Kuhlbrandt W (2017). Cryo-EM structure of the TOM core complex from Neurospora crassa. Cell 170, 693–700.e697.

Bhagawati M, Hoffmann S, Hoffgen KS, Piehler J, Busch KB, Mootz HD (2020). Cellulo protein semi-synthesis from endogenous and exogenous fragments using the ultra-fast split Gp41-1 Intein. Angew Chem Int Ed Engl 59, 2–11.

Brix J, Ziegler GA, Dietmeier K, Schneider-Mergener J, Schulz GE, Pfanner N (2000). The mitochondrial import receptor Tom70: identification of a 25 kDa core domain with a specific binding site for preproteins. J Mol Biol 303, 479–488.

Bykov YS, Rapaport D, Herrmann JM, Schuldiner M (2020). Cytosolic events in the biogenesis of mitochondrial proteins. Trends Biochem Sci 45, 650–667.

Carvajal-Vallejos P, Pallisse R, Mootz HD, Schmidt SR (2012). Unprecedented rates and efficiencies revealed for new natural split inteins from metagenomic sources. J Biol Chem 287, 28686–28696.

Claros MG, Vincens P (1996). Computational method to predict mitochondrially imported proteins and their targeting sequences. Eur J Biochem 241, 779–786.

Dekker PJ, Ryan MT, Brix J, Muller H, Honlinger A, Pfanner N (1998). Preprotein translocase of the outer mitochondrial membrane: molecular dissection and assembly of the general import pore complex. Mol Cell Biol 18, 6515–6524.

Gornicka A, Bragoszewski P, Chroscicki P, Wenz LS, Schulz C, Rehling P, Chacinska A (2014). A discrete pathway for the transfer of intermembrane space proteins across the outer membrane of mitochondria. Mol Biol Cell 25, 3999–4009.

Heijne G (1986). The distribution of positively charged residues in bacterial inner membrane proteins correlates with the trans-membrane topology. EMBO J 5, 3021–3027.

Jaqaman K, Loerke D, Mettlen M, Kuwata H, Grinstein S, Schmid SL, Danuser G (2008). Robust single-particle tracking in live-cell time-lapse sequences. Nat Methods 5, 695–702.

Kondadi AK, Anand R, Hansch S, Urbach J, Zobel T, Wolf DM, Segawa M, Liesa M, Shirihai OS, Weidtkamp-Peters S, *et al*. (2020). Cristae undergo continuous cycles of membrane remodelling in a MICOS-dependent manner. EMBO Rep 21, e49776.

Kuzmenko A, Tankov S, English BP, Tarassov I, Tenson T, Kamenski P, Elf J, Hauryliuk V (2011). Single molecule tracking fluorescence microscopy in mitochondria reveals highly dynamic but confined movement of Tom40. Sci Rep 1, 195.

Lisse D, Wilkens V, You C, Busch K, Piehler J (2011). Selective targeting of fluorescent nanoparticles to proteins inside live cells. Angew Chem Int Ed Engl 50, 9352–9355.

Meisinger C, Brix J, Model K, Pfanner N, Ryan MT (1999). The preprotein translocase of the outer mitochondrial membrane: receptors and a general import pore. Cell Mol Life Sci 56, 817–824.

Model K, Prinz T, Ruiz T, Radermacher M, Krimmer T, Kuhlbrandt W, Pfanner N, Meisinger C (2002). Protein translocase of the outer mitochondrial membrane: role of import receptors in the structural organization of the TOM complex. J Mol Biol 316, 657–666.

Mootha VK, Bunkenborg J, Olsen JV, Hjerrild M, Wisniewski JR, Stahl E, Bolouri MS, Ray HN, Sihag S, Kamal M, *et al*. (2003). Integrated analysis of protein composition, tissue diversity, and gene regulation in mouse mitochondria. Cell 115, 629–640.

Morgenstern M, Stiller SB, Lubbert P, Peikert CD, Dannenmaier S, Drepper F, Weill U, Hoss P, Feuerstein R, Gebert M, *et al*. (2017). Definition of a high-confidence mitochondrial proteome at quantitative scale. Cell Rep 19, 2836–2852.

Rapaport D (2002). Biogenesis of the mitochondrial TOM complex. Trends Biochem Sci 27, 191–197.

Sakaue H, Shiota T, Ishizaka N, Kawano S, Tamura Y, Tan KS, Imai K, Motono C, Hirokawa T, Taki K, *et al*. (2019). Porin associates with Tom22 to regulate the mitochondrial protein gate assembly. Mol Cell 73, 1044–1055.e1048.

Salewskij K, Rieger B, Hager F, Arroum T, Duwe P, Villalta J, Colgiati S, Richter CP, Psathaki OE, Enriquez JA, *et al*. (2020). The spatio-temporal organization of mitochondrial F1FO ATP synthase in cristae depends on its activity mode. Biochim Biophys Acta Bioenerg 1861, 148091.

Shiota T, Imai K, Qiu J, Hewitt VL, Tan K, Shen HH, Sakiyama N, Fukasawa Y, Hayat S, Kamiya M, *et al*. (2015). Molecular architecture of the active mitochondrial protein gate. Science 349, 1544–1548.

Shiota T, Mabuchi H, Tanaka-Yamano S, Yamano K, Endo T (2011). In vivo protein-interaction mapping of a mitochondrial translocator protein Tom22 at work. Proc Natl Acad Sci USA 108, 15179–15183.

Sohnel AC, Kohl W, Gregor I, Enderlein J, Rieger B, Busch KB (2016). Probing of protein localization and shuttling in mitochondrial microcompartments by FLIM with sub-diffraction resolution. Biochim Biophys Acta 1857, 1290–1299.

STRING-consortium (2020). Functional partners of Tom20 in Pongo abelii. (internet, ELIXIR's Core Data Resources).

Tokunaga M, Imamoto N, Sakata-Sogawa K (2008). Highly inclined thin illumination enables clear single-molecule imaging in cells. Nat Methods 5, 159–161.

Volkmann G, Mootz HD (2013). Recent progress in intein research: from mechanism to directed evolution and applications. Cell Mol Life Sci 70, 1185–1206.

Wang W, Chen X, Zhang L, Yi J, Ma Q, Yin J, Zhuo W, Gu J, Yang M. (2020). Atomic structure of human TOM core complex. Cell Discov 6, 67.

Wiedemann N, Pfanner N (2017). Mitochondrial machineries for protein import and assembly. Annu Rev Biochem 86, 685–714.

Wittig I, Carrozzo R, Santorelli FM, Schagger H (2006). Supercomplexes and subcomplexes of mitochondrial oxidative phosphorylation. Biochim Biophys Acta 1757, 1066–1072.

Wittig I, Karas M, Schagger H (2007). High resolution clear native electrophoresis for in-gel functional assays and fluorescence studies of membrane protein complexes. Mol Cell Proteomics 6, 1215–1225.

Yu T, Fox RJ, Burwell LS, Yoon Y (2005). Regulation of mitochondrial fission and apoptosis by the mitochondrial outer membrane protein hFis1. J Cell Sci 118, 4141–4151.